

# Effect of a humid environment on the surface structure of RuO<sub>2</sub>(110)

Qiang Sun, Karsten Reuter and Matthias Scheffler

*Fritz-Haber-Institut der Max-Planck-Gesellschaft, Faradayweg 4-6, D-14195 Berlin, Germany*

(Dated: Received 29 July 2002)

Combining density-functional theory and thermodynamics we compute the phase diagram of surface structures of rutile RuO<sub>2</sub>(110) in equilibrium with water vapor in the complete range of experimentally accessible gas phase conditions. Through the formation of hydroxyl or water-like groups, already lowest concentrations of hydrogen in the gas phase are sufficient to stabilize an oxygen-rich polar oxide termination even at very low oxygen pressure.

PACS numbers: PACS: 68.47.Gh, 05.70.Np, 71.15.Mb

## I. INTRODUCTION

Metal oxides are employed in a wide range of technological applications, as for example catalysis (where they may serve as the support or the active material) and corrosion or wear protection in mechanical systems. A microscopic understanding of the function of these compounds requires knowledge of their often complex surface atomic structures,<sup>1,2</sup> which may be sensitively influenced by temperature and partial pressures in the surrounding environment. This dependence could be particularly prominent in oxygen-containing environments, where oxide terminations of varying stoichiometry are easily perceived as a function of the abundance of oxygen in the surrounding. The situation becomes even more complicated by realizing that also hydrogen is almost always present in real-life systems, e.g., as a species in the reactant feed gas or as a bulk impurity. Then, it is in fact very plausible that surfaces are terminated by hydroxyl groups, as has recently been exemplified by Wang *et al.* for the  $\alpha$ -Al<sub>2</sub>O<sub>3</sub>(0001) surface.<sup>3</sup>

Although it is quite obvious that such variations in the oxide surface structure and composition may affect the function of these materials in applications, systematic studies analyzing this issue are surprisingly sparse, even for well-defined oxide surfaces.<sup>1,2</sup> To this end we describe in the following how the method of *first-principles atomistic thermodynamics*<sup>3-10</sup> can be employed to construct a phase diagram of the most stable surface structures of an arbitrary oxide surface in equilibrium with its environment in the complete range of experimentally accessible temperature and pressure conditions. As specific example we choose the RuO<sub>2</sub>(110) surface in contact with a humid gas phase formed of hydrogen and oxygen. Recent experiments have not only shown this surface to be an efficient CO oxidation catalyst<sup>11,12</sup>, but also a sensitive dependence of the measured turnover rate on the amount of hydrogen present in the system was reported<sup>13</sup>. In these measurements, RuO<sub>2</sub>(110) showed a particularly high reactivity for the low temperature oxidation of CO by humid air, i.e. conditions where most technological catalysts cannot be applied due to anodic corrosion<sup>13</sup>. This renders this oxide an interesting object of study de-

spite its problematic technological applicability due to the poisonous nature of Ru.

Similar to the results obtained by Wang *et al.* for  $\alpha$ -Al<sub>2</sub>O<sub>3</sub>(0001)<sup>3</sup> we show in the following that also for RuO<sub>2</sub>(110) already lowest amounts of hydrogen in the gas phase lead to an overwhelming stability of hydrogenated surface phases. Through the formation of hydroxyl or water-like groups an oxygen-rich polar oxide termination is then stabilized over the complete range of accessible oxygen pressures. Concomitantly, the strength of the O-H bonds formed is so high, that even in ultra-high vacuum (UHV) annealing temperatures of the order of 600 K will be required to fully remove hydrogen from this transition-metal (TM) oxide surface. While this not only indicates the danger of unintentional hydrogen contamination in *Surface Science* experiments, our findings also demonstrate the sensitive dependence of oxide surface structure and composition on the surrounding gas phase. The latter should be systematically taken into account when addressing the functionality of these surfaces in technical applications.

## II. THEORY

In equilibrium with a given environment, characterized by temperature,  $T$ , and partial pressures,  $\{p_i\}$ , the stable surface structure minimizes the surface free energy, defined as

$$\gamma(T, \{p_i\}) = \frac{1}{A} [G(T, \{p_i\}, N_i) - \sum_i N_i \mu_i(T, p_i)].$$

Here,  $G(T, \{p_i\}, N_i)$  is the Gibbs free energy of the finite crystal,  $N_i$  and  $\mu_i(T, p_i)$  are number and chemical potential of the species of  $i$ th type, and  $\gamma(T, \{p_i\})$  is normalized to energy per unit area by dividing through the surface area  $A$ . In the present application to RuO<sub>2</sub>(110) in contact with a gas phase containing oxygen and hydrogen, the surface free energy is thus a function of the three chemical potentials of Ru, O, and H. Assuming that the surface is also in equilibrium with the underlying oxide bulk constrains the chemical potentials of the two oxide components, as their stoichiometric sum has then

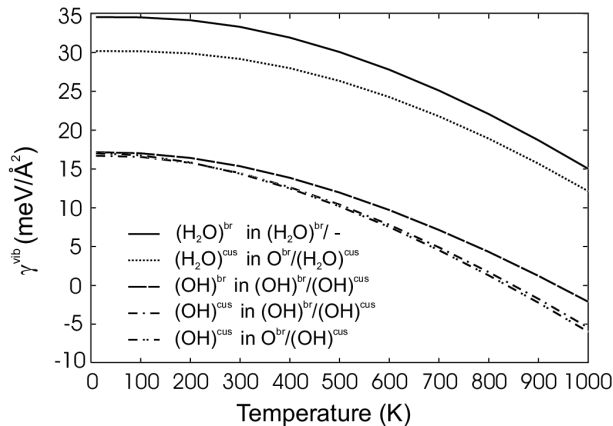


FIG. 1: Vibrational contribution of surface hydrogen groups to the surface free energy of various hydrogenated phases of  $\text{RuO}_2(110)$ . See text for an explanation of the nomenclature used to describe the individual phases.

to equal the Gibbs free energy of the bulk oxide. As a consequence the surface free energy can be discussed just in terms of a dependence on  $\mu_{\text{O}}$  and  $\mu_{\text{H}}$ , which are both determined by the surrounding gas phase reservoirs and thus directly related to the experimentally controllable parameters, temperature and partial pressure<sup>9,14</sup>.

We also note that not the absolute value of  $G(T, \{p_i\}, N_i)$  enters the calculation of  $\gamma(T, \{p_i\})$ , but only the difference of the surface and the bulk Gibbs free energies. In ref. 9 we could show that for  $\text{RuO}_2(110)$  in an oxygen environment the vibrational and entropic contributions to this difference,  $\gamma_{\text{RuO}_2}^{\text{vib.}}(T)$ , cancel to a large degree. This does, however, not comprise the contributions from adsorbate functional groups. Since they have no counterpart in the bulk Gibbs free energy, their absolute vibrational energy and entropy enters into a contribution  $\gamma^{\text{vib.}}(T)$  to the surface free energy of the corresponding phase<sup>9</sup>. In most cases involving atomic or small molecular adsorbates this extra-contribution is fortunately still negligible within our aspired accuracy of  $\pm 10 - 15 \text{ meV}/\text{\AA}^2$ , as there is only a limited number of (low-energy) vibrational modes that gives rise to it.

Due to their high-energy modes, hydrogen functional groups form a notable exception to this line of thought, yielding rather high  $\gamma^{\text{vib.}}(T)$  already for hydroxyl groups or water-like species at the surface. This is illustrated in Fig. 1 for various such phases discussed later in the text. The  $\gamma^{\text{vib.}}(T)$  have been obtained from a detailed vibrational analysis of the various surface species, diagonalizing the complete dynamic matrix while leaving the substrate fixed<sup>16</sup>. We see that for  $T < 700 \text{ K}$   $\gamma^{\text{vib.}}(T)$  is of the order of  $15 \text{ meV}/\text{\AA}^2$  for hydroxyl groups and of the order of  $30 \text{ meV}/\text{\AA}^2$  for water-like adspecies. Interestingly, there is little variation in these values, when the functional groups adsorb in different surface sites, or even coadsorb closely to each other (see text below for the specific nomenclature employed to describe the individual

TABLE I: Experimental and theoretical binding energies,  $E_{\text{b}}$ , as well as vibration frequencies of isolated  $\text{H}_2$ ,  $\text{O}_2$  and  $\text{H}_2\text{O}$  molecules. The theoretical values are obtained within our DFT-GGA approach using the same basis set that is also employed in the slab computations.

		$E_{\text{b}}$	$\nu_{\text{stretch}}$ (sym/asym)	$\nu_{\text{scissor}}$
$\text{H}_2$	exp	4.52 eV/mol. <sup>21</sup>	546 meV <sup>17</sup>	--
	theory	4.50 eV/mol.	538 meV	--
$\text{O}_2$	exp	5.16 eV/mol. <sup>21</sup>	193 meV <sup>22</sup>	--
	theory	5.86 eV/mol.	180 meV	--
$\text{H}_2\text{O}$	exp	9.60 eV/mol. <sup>23</sup>	454/466 meV <sup>17</sup>	198 meV <sup>17</sup>
	theory	9.81 eV/mol.	424/435 meV	189 meV

surface phases). Very similar  $\gamma^{\text{vib.}}(T)$  are also obtained if we use typical vibrational modes of these two surface functional groups when adsorbed on metallic surfaces<sup>17</sup>. Although the individual modes change, these variations have apparently little effect on the composite quantity  $\gamma^{\text{vib.}}(T)$ . Furthermore, if we restrict our discussion to  $T < 700-800 \text{ K}$ , also the temperature-dependence of this vibrational contribution to the surface free energy becomes very small, cf. Fig. 1. Correspondingly, we may approximately take it into account by simply adding a constant  $\gamma^{\text{vib.}}$  of  $15 \text{ meV}/\text{\AA}^2$  per present hydroxyl-group and  $30 \text{ meV}/\text{\AA}^2$  per present water-like species in the computation of the  $\gamma(T, \{p_i\})$  of corresponding hydrogenated surface phases.

Not aiming at an accuracy better than the stated  $10-15 \text{ meV}/\text{\AA}^2$ , we may then replace the two free energies entering  $\gamma(T, \{p_i\})$  by their total energies, and calculate them using density-functional theory within the full-potential linear augmented plane wave (FP-LAPW) approach<sup>18</sup> and the generalized gradient approximation (GGA) for the exchange-correlation functional<sup>19</sup>. The high accuracy of the basis set<sup>20</sup> employed in these supercell calculations has been detailed in a preceding publication that discussed the stability of  $\text{RuO}_2(110)$  in a pure oxygen environment<sup>9</sup>. Thus, the numerical accuracy of differences between  $\gamma(T, \{p_i\})$  values of different surface structures is better than  $\pm 5 \text{ meV}/\text{\AA}^2$ , while we stress that the aforementioned approximate treatment of vibrational and entropic contributions does not allow to distinguish between phases which  $\gamma(T, \{p_i\})$  differ by less than about  $10-15 \text{ meV}/\text{\AA}^2$ . In comparison to our previous work we were forced to reduce the oxygen muffin-tin radius to 1 bohr, in order to treat the short O-H bonds in the present extension to a gas phase containing both oxygen and hydrogen. Consequently we had to increase the plane wave cutoff in the interstitial region from 17 Ry to 20.25 Ry for the wavefunctions and from 169 Ry to 400 Ry for the potential to maintain the same level of accuracy. Otherwise the same set-up is used for our computations as detailed before<sup>9</sup>.

To further assess our ability to properly describe particularly the energetics of O-H bonds within our DFT-GGA approach, we computed the binding energy, as well

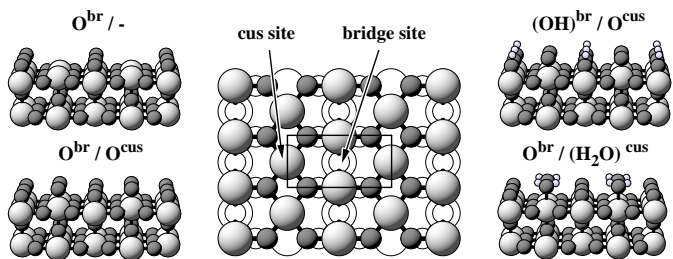


FIG. 2: Top view of the  $\text{RuO}_2(110)$  surface explaining the location of the two prominent adsorption sites (bridge and cus), which continue the bulk-stacking sequence (central panel). Additionally shown are perspective views of the two most stable  $(1 \times 1)$  terminations involving only O (left panel). The geometry of hydrogenated surfaces is exemplified for two cases, comprising once a hydroxyl group at the bridge site (top right) and once adsorbed water at the cus site (bottom right). See text for explanation of the short hand notation used to describe the various surface phases. Ru = light, large spheres, O = dark, medium spheres, H = white, small spheres.

as vibration frequencies of free  $\text{H}_2$  and  $\text{H}_2\text{O}$  molecules in the gas phase by diagonalizing their dynamic matrix. The results are compiled in Table I and compared to our results for molecular  $\text{O}_2$ . In contrast to the known strong overbinding in the latter case<sup>19</sup>, the hydrogen-related results show close agreement with reported experimental values. With a procedure described in detail in our previous publication<sup>9</sup>, we can significantly reduce the large error introduced into the computed surface free energy due to the oxygen overbinding, giving us finally good confidence that the chosen set-up is adequate. Checking especially on the approximate nature of the exchange-correlation functional we additionally repeated the most relevant computations entering into the construction of the surface phase diagram within the local-density approximation (LDA)<sup>24</sup> and will comment on these findings in the discussion below.

### III. SURFACE STRUCTURE OF $\text{RuO}_2(110)$

$\text{RuO}_2(110)$  has recently attracted considerable interest as playing a key role in the catalytic CO oxidation at a  $\text{Ru}(0001)$  surface that is exposed to high oxygen pressure.<sup>9-12,25-31</sup> The atomic arrangement of this rutile (110) surface, also known from  $\text{TiO}_2(110)$ , exhibits two distinct adsorption sites within the computed  $(6.43 \text{ \AA} \times 3.12 \text{ \AA})$  rectangular surface unit-cell. Figure 2 shows these two prominent sites over the oxygen-poor termination of  $\text{RuO}_2(110)$ : The so-called coordinatively unsaturated (cus) site (atop of fivefold coordinated Ru atoms,  $\text{Ru}^{\text{cus}}$ ), and the bridge (br) site between two fourfold coordinated Ru atoms ( $\text{Ru}^{\text{br}}$ ). The bulk stacking sequence would be continued by oxygen atoms first occupying the bridge ( $\text{O}^{\text{br}}$ ) and then the cus ( $\text{O}^{\text{cus}}$ ) sites, thus leading to the two other  $(1 \times 1)$  terminations of a rutile (110)

surface shown in perspective view in the left panels of Fig. 2, cf. ref. 9 for more details.

To evaluate the surface phase diagram we computed what we believe are all possible  $(1 \times 1)$  (co-)adsorption geometries of O and H at the cus and bridge sites of  $\text{RuO}_2(110)$ . Additionally, we also considered any possible combination of adsorbed molecular  $\text{H}_2$ , OH, and  $\text{H}_2\text{O}$  groups at these two adsorption sites. In the following we will use a short hand notation to characterize this manifold of studied geometries, indicating first the occupancy of the bridge site and then of the cus site, e.g.  $(\text{OH})^{\text{br}}/-$  for an OH-group at the bridge site, the cus site being empty, cf. Fig. 2. Although adsorption of H or O is in principle also conceivable at other sites on the surface, test calculations always resulted in significantly lower binding energies compared to adsorption at the cus or bridge sites. Correspondingly, we may restrict our discussion to these two prominent sites in the following. In view of the more than 20 studied geometries we would like to emphasize at this point that a complete structural relaxation - including symmetry breaking at the surface - was essential to obtain the correct energetics, as we find particularly the tilting of OH and water-like groups to decisively influence the relative stabilities of the tested geometries.

Our self-consistent DFT total energies implicitly contain all lateral interactions within the considered  $(1 \times 1)$  surface unit-cell. Significant lateral interactions beyond the first-neighbor cus-br interaction, cf. Fig. 2, could e.g. lead to ordered adsorption phases that are more dilute. For pure oxygen phases we therefore performed a systematic study to extract all lateral interactions between adsorbed oxygen atoms employing large surface unit-cells up to  $(4 \times 1)$  and  $(2 \times 2)$  periodicity<sup>32</sup>. We found only very small lateral interactions, which we understand being a consequence of the rather open surface structure (compared to the more often studied close-packed metal surfaces). We don't expect this picture to change significantly in the case of H and O coadsorption, as confirmed by a series of test calculations employing  $(2 \times 1)$  surface unit-cells. The remaining small lateral interactions or disorder effects will only affect the relative stabilities close to the boundaries between different stable phases. In the present study we aim to construct the large scale phase diagram in the whole range of experimentally accessible gas phase parameters. Small variations in the vicinity of the obtained phase boundaries do not change the physical conclusions we deduce on the basis of this phase diagram and are thus not of present concern. Hence, we will restrict the discussion here to the (still large) number of  $(1 \times 1)$  geometries and defer a systematic study of larger unit-cell phases to a forthcoming publication.

#### IV. SURFACE PHASE DIAGRAM OF HYDROGENATED $\text{RuO}_2(110)$

When now discussing the dependence of the computed surface free energies on the chemical potentials of the gas phase species, we note that experimentally (and assuming that thermodynamic equilibrium applies)  $\mu_{\text{O}}$  cannot be varied without bounds. If it gets too low, all lattice oxygen atoms would preferably go into the gas phase, i.e. the oxide would decompose. On the other hand, if  $\mu_{\text{O}}$  gets too high, oxygen will start to condense on the surface. Theoretical estimates for both extremes can be derived<sup>9</sup> and we will correspondingly restrict the presentation of the surface free energies to the limited range between this O-poor and O-rich boundary, respectively.

Extending this to a multi-component environment we note that depending on the gas phase reaction barrier(s) an equilibrium composition may or may not be present in the gas phase. If the barrier is rather high, as in the case of the CO oxidation reaction, the *first-principles atomistic thermodynamics* concept can e.g. be employed to address the situation of a *constrained equilibrium* where each gas phase species is separately in equilibrium with the surface, but not with the respective other gas component(s). Depending on the reaction barriers for the adsorbed species, surface kinetic effects may then become important for certain temperature and pressure conditions, so that the actual surface structure deviates from the prediction of the thermodynamic approach<sup>10</sup>.

This problem does not arise, if one concentrates on the situation where the environment is itself fully equilibrated. In the present context of a gas phase containing oxygen and hydrogen this corresponds to allowing for the possibility of water formation in the oxyhydrogen reaction. In fact, over the whole finite stability range possible over  $\text{RuO}_2(110)$ ,  $\mu_{\text{O}}$  is already so high that water is not only a possibility, but the dominant gas phase component, if such a full equilibrium is reached<sup>3</sup>. *Modelling this particular situation*, the chemical potential of hydrogen atoms at the  $\text{RuO}_2(110)$  surface is therefore determined by a  $\text{H}_2\text{O}$  reservoir in the following. To assure that we restrict the discussion to a humid environment, i.e. stay within the gaseous state of water for any temperature or pressure, the maximum  $\mu_{\text{H}_2\text{O}}$  considered will be at  $-0.91$  eV with respect to the total energy of a  $\text{H}_2\text{O}$  molecule, which corresponds to the chemical potential of water at the (experimental) critical point.<sup>14</sup>

Before addressing the equilibrium with the two component gas phase, it is instructive to first discuss the oxide surface structure in a pure  $\text{O}_2$  atmosphere<sup>9</sup>. Then, the surface free energy depends only on the chemical potential of oxygen, which in turn represents the two-dimensional dependence on temperature and oxygen pressure. Figure 3 shows the limited stability range between the O-poor and O-rich boundary. To make the dependence on  $\mu_{\text{O}}$  a bit more lucid, we additionally show a pressure scale in the top  $x$ -axis for fixed  $T = 600\text{K}$ , which is a typical annealing temperature employed in

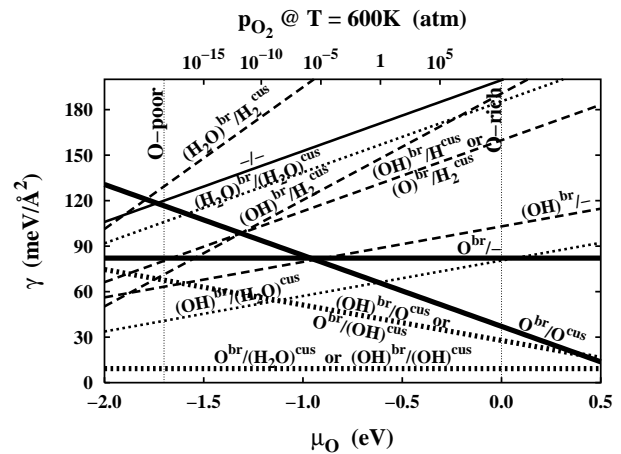


FIG. 3: Surface free energies of the three  $(1 \times 1)$ - $\text{RuO}_2(110)$  terminations involving only oxygen (solid lines). The corresponding  $\gamma(T, \{p_i\})$  of hydrogen containing phases are drawn with dashed lines, if no O is present at the cus sites, and with dotted lines, if O is present (see Fig. 2 for nomenclature and site explanation). The dotted vertical lines indicate the allowed range of oxygen chemical potential, while the chemical potential of H is in this plot chosen for very H-rich conditions corresponding to the experimental critical point of water ( $\mu_{\text{H}_2\text{O}} = -0.91 \text{ eV}^{14}$ ). In the top  $x$ -axis, the dependence on  $\mu_{\text{O}}(T, p_{\text{O}_2})$  has been cast into a pressure scale at a fixed temperature of  $T = 600\text{K}$ .

this system<sup>11,12</sup>. The solid lines indicate the surface free energies of the three possible  $(1 \times 1)$  terminations of a rutile  $(110)$  surface. While the mixed O-Ru termination, where both cus and bridge sites are unoccupied  $(-/-)$ , is rather high up in energy, the two lines corresponding to the other two terminations displayed in Fig. 3 intersect in about the middle of the possible range of oxygen chemical potential. At lower  $\mu_{\text{O}}$ , corresponding to ultrahigh vacuum (UHV) conditions, the traditionally discussed stoichiometric termination is stable, where oxygen occupies only the bridge sites at the surface ( $\text{O}^{\text{br}}/-$ ). However, towards higher oxygen pressures we find a second, O-rich termination to become more stable, in which  $\text{O}^{\text{cus}}$  atoms are now also present ( $\text{O}^{\text{br}}/\text{O}^{\text{cus}}$ ).

When next addressing the equilibrium with a gas phase containing additionally water vapor, the one-dimensional dependence of the surface free energy on  $\mu_{\text{O}}$  gets extended to the two-dimensional dependence on  $(\mu_{\text{O}}, \mu_{\text{H}_2\text{O}})$ . The maximum effect of the additional gas component on the surface structure can be seen from the surface free energies of hydrogenated geometries in the upper H-rich limit of  $\mu_{\text{H}_2\text{O}}$  described above<sup>14</sup>. For this particular chemical potential ( $\mu_{\text{H}_2\text{O}} = -0.91 \text{ eV}$ ) the lines corresponding to the most stable structures studied are included in Fig. 3: Dotted lines represent geometries including  $\text{O}^{\text{cus}}$  atoms, while dashed lines depict phases, where no oxygen is present at the cus sites. Interestingly, we find several cases, where different surface geometries of identical stoichiometry, which correspondingly exhibit

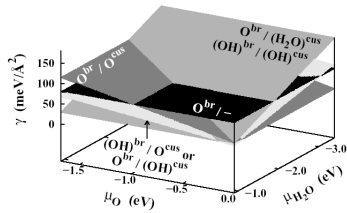


FIG. 4: Surface free energies of the four stable phases (or degenerate phase pairs) discussed in the text, as a function of  $(\mu_{\text{O}}, \mu_{\text{H}_2\text{O}})$ . The corresponding phases are drawn as thick lines in Fig. 3 for the H-rich limit.

parallel  $\gamma(T, \{p_i\})$  lines in Fig. 3, turn out energetically virtually degenerate, i.e. their surface free energies within DFT-GGA differ by less than  $\pm 5 \text{ meV}/\text{\AA}^2$  and are thus not distinguishable within the approximations of our approach described above. In such cases we only include one line in the graph and label it with both geometries.

Particularly relevant for the future discussion will be the two thicker drawn dotted lines, each representing a degenerate pair of surface phases. In the first case, two H atoms are present per  $(1 \times 1)$  surface unit-cell, forming either a chemisorbed water-like species at the cus sites ( $\text{O}^{\text{br}}/(\text{H}_2\text{O})^{\text{cus}}$ ) or hydroxyl groups at both bridge and cus sites ( $(\text{OH})^{\text{br}}/(\text{OH})^{\text{cus}}$ ). In the second case, one H atom per unit-cell forms a hydroxyl group either at the bridge or at the cus site ( $(\text{OH})^{\text{br}}/\text{O}^{\text{cus}}$  and  $\text{O}^{\text{br}}/(\text{OH})^{\text{cus}}$  respectively), cf. Fig. 2. We note that particularly the virtual degeneracy of these last two phases is somewhat surprising, as they correspond to quite different geometries, namely to bridge-bonded and atop-bonded OH-groups at different surface sites. As apparent from Fig. 3, the surface free energy in this H-rich limit is significantly lowered in both cases (thick dotted lines) in comparison to the two stable pure O terminations (thick solid lines) discussed before.

Allowing variations of  $\mu_{\text{H}_2\text{O}}$  away from the H-rich limit, the two-dimensional graph in Fig. 3 turns into the three-dimensional one shown in Fig. 4, where we now only include the surface free energy planes of the four most stable phases (or degenerate phase pairs), that will play a role in the later discussion. Note that at the maximum  $\mu_{\text{H}_2\text{O}} = -0.91 \text{ eV}$  along the front  $x$ -axis in Fig. 4 we simply recover the two-dimensional dependence of Fig. 3. While the  $\gamma(T, \{p_i\})$  of the two pure O terminations,  $\text{O}^{\text{br}}/-$  and  $\text{O}^{\text{br}}/\text{O}^{\text{cus}}$ , do, of course, not depend on  $\mu_{\text{H}_2\text{O}}$ , the hydrogenated geometries become increasingly less favorable the lower the water chemical potential becomes, i.e. the less hydrogen is present in the gas phase. For the lowest  $\mu_{\text{H}_2\text{O}}$  shown in Fig. 4, all H involving phases have then already become less stable than the pure O terminations for any  $\mu_{\text{O}}$ , i.e. the H content in the gas phase is so low, that no hydrogen can be stabilized at the surface anymore.

Although instructive, the three-dimensional presentation does not allow an easy access to the most relevant

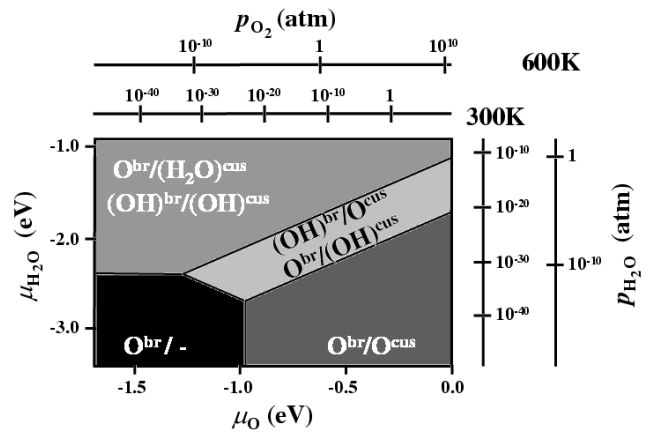


FIG. 5: Surface phase diagram of stable structures of  $\text{RuO}_2(110)$  in equilibrium with a humid environment, i.e. as a function of  $(\mu_{\text{O}}, \mu_{\text{H}_2\text{O}})$  in the gas phase. The additional axes show the corresponding pressure scales at  $T = 300 \text{ K}$  and  $600 \text{ K}$ .

information contained in Fig. 4, namely which phase has the lowest surface free energy for given gas-phase conditions, i.e. given  $(\mu_{\text{O}}, \mu_{\text{H}_2\text{O}})$ . Therefore we display in Fig. 5 this surface phase diagram of stable structures, which corresponds to taking a look at Fig. 4 from below. We find all four phases (or degenerate phase pairs) discussed up to now to be most stable in different  $(\mu_{\text{O}}, \mu_{\text{H}_2\text{O}})$ -regions: At the lowest  $\mu_{\text{H}_2\text{O}}$  shown so little hydrogen is present in the environment, that just the surface structure dependence of  $\text{RuO}_2(110)$  in a pure  $\text{O}_2$  atmosphere is recovered, i.e. the stoichiometric  $\text{O}^{\text{br}}/-$  phase is stable at low  $\mu_{\text{O}}$ , while towards higher oxygen pressures,  $\text{O}^{\text{cus}}$  is additionally stabilized leading to the  $\text{O}^{\text{br}}/\text{O}^{\text{cus}}$  phase. Upon increasing the H content in the gas phase hydrogen first forms one hydroxyl group per surface unit-cell ( $(\text{OH})^{\text{br}}/\text{O}^{\text{cus}}$  or  $\text{O}^{\text{br}}/(\text{OH})^{\text{cus}}$ ), whereas towards H-rich and O-poor conditions in the upper left part of Fig. 5 the maximum coverage of two H atoms per surface unit-cell is reached. This leads either to two hydroxyl groups at both bridge and cus sites ( $(\text{OH})^{\text{br}}/(\text{OH})^{\text{cus}}$ ) or to a chemisorbed water-like species, bound with 1eV to the cus sites as shown in the right bottom panel of Fig. 2 ( $\text{O}^{\text{br}}/(\text{H}_2\text{O})^{\text{cus}}$ ).

In order to check how much our results may be affected by the exchange-correlation functional, we recomputed the stable surface phases using the LDA, i.e. considering the LDA lattice constant for the substrate ( $6.45 \text{ \AA} \times 3.16 \text{ \AA}$ ) and including a full geometry reoptimization. Although the absolute surface free energies are found to be on average about  $\approx 15 \text{ meV}/\text{\AA}^2$  higher compared to the DFT-GGA results, the same energetic sequence as displayed in Fig. 3 was obtained. In particular, the two pairs of degenerate surface structures discussed before give again surface free energies differing by less than  $15 \text{ meV}/\text{\AA}^2$  from each other and thus exhibit stabilities that cannot be distinguished within the current approx-

imations. Correspondingly, the phase diagram obtained within the LDA exhibits the same four stable regions and the same qualitative structure as the one shown in Fig. 5. Quantitatively, the phase boundaries of the hydrogenated phases are shifted by about 0.5 eV towards lower  $\mu_{\text{H}_2\text{O}}$ , indicating that hydrogen bonds are stronger within the LDA. In line with our preceding study<sup>9</sup> we therefore conclude that the uncertainty in the DFT exchange-correlation functional may affect transition temperatures or pressures between stable phases deduced on the basis of the constructed phase diagrams. Yet the transitions *per se*, i.e. the overall structure of the phase diagram, are not changed.

To translate the dependence on the chemical potentials into temperature and pressure, the pressure scales at room temperature and  $T = 600$  K are also included in Fig. 5. From those we can derive e.g. what pressures would be required in the gas phase in order to stabilize hydrogen at RuO<sub>2</sub>(110). The transition from the pure O terminations to the H involving phases at somewhat academic hydrogen pressures of the order of  $10^{-30}$  atm for  $T = 300$  K simply indicates that the oxide surface will always be hydrogenated at this low temperature in any realistic environment, or in other words that the other areas of the phase diagram are experimentally not accessible at  $T=300$  K. From our results we can further conclude, that even under UHV conditions, temperatures of the order of 500-600 K (GGA, or 600-700 K within the LDA) would be required to remove hydrogen completely from the surface, while at atmospheric pressure this rises to about 1000 K, i.e. to temperatures already close to the decomposition of the whole oxide. It is interesting to notice that in a number of recent experimental studies on RuO<sub>2</sub>(110) an annealing temperature of only  $T = 600$  K was employed<sup>11,12,28</sup>. According to our results this might not have been sufficient to completely remove residual H contaminants from the surface. Similarly, our results also imply that hydrogen has to be taken into account as a likely surface species under all realistic gas phase conditions up to rather elevated temperatures, e.g. also in all catalytically-relevant environments.

## V. COMPARISON WITH HYDROGENATED $\alpha$ -Al<sub>2</sub>O<sub>3</sub>

The phase diagram in Fig. 5 reveals that the most notable effect of hydrogenation is to stabilize O<sup>cus</sup> atoms over the complete range of possible oxygen pressure: While in the pure O<sub>2</sub> atmosphere the phase including O<sup>cus</sup> becomes only more stable towards higher oxygen chemical potentials, this species is present in all four stable hydrogenated phases for any  $\mu_{\text{O}}$  at sufficiently high  $\mu_{\text{H}_2\text{O}}$ , cf. Fig. 5. In other words, already lowest concentrations of hydrogen in the gas phase are sufficient to stabilize a non-stoichiometric surface terminated by either hydroxyl groups (one H at O) or water-like species (two H at O). This finding is analogous to the results on  $\alpha$ -

Al<sub>2</sub>O<sub>3</sub>(0001) obtained by Wang *et al.*<sup>3</sup>, who reported the purely hydrogen-induced stability of the O-rich O-plane termination of this corundum structure. Yet, while in the latter case the polar termination is never favorable without the presence of hydrogen, a humid environment only increases the stability range of the O-rich surface (in terms of hydroxyl groups) in the case of RuO<sub>2</sub>(110).

The hydrogenation goes in both cases hand in hand with a drastic reduction of the work function. For RuO<sub>2</sub>(110) adding the O<sup>cus</sup> atoms first significantly increases the work function by +1.5 eV, reflecting the increased dipole moment of the O-rich O<sup>br</sup>/O<sup>cus</sup> termination<sup>9</sup>. On the contrary, adding hydrogen into the surface geometry markedly reduces the work function again by -2.0 eV or -3.5 eV for the phases involving one or two hydroxyl groups, respectively. On  $\alpha$ -Al<sub>2</sub>O<sub>3</sub>, which was found to stabilize up to three hydroxyl groups per surface unit-cell, even larger work function reductions by more than 6 eV were obtained<sup>3</sup>.

Unfortunately it is not clear, whether the latter 3H per cell coverage corresponds already to full saturation, as the possibility of water-like species was not considered in the study by Wang *et al.*<sup>3</sup> Nevertheless, already for the fully hydroxylated  $\alpha$ -Al<sub>2</sub>O<sub>3</sub>(0001) surface negative surface free energies were obtained in the H-rich limit, indicating the strength of the H-OAl bond and consistent with the negative heat of the  $\alpha$ -Al<sub>2</sub>O<sub>3</sub> + 3H<sub>2</sub>O → 2Al(OH)<sub>3</sub> reaction<sup>3</sup>. On the other hand, the weaker H-ORu bond never leads to negative  $\gamma(T, \{p_i\})$  even at the most H-rich conditions, cf. Fig. 3. This lower bond strength is also reflected by the result that the fully hydroxylated RuO<sub>2</sub>(110) surface still exhibits a compression of the topmost layer distance, although this compression is noticeably reduced compared to the hydrogen free surface. In contrast it had been found that the topmost layer is already strongly relaxed outwards at the fully hydroxylated corundum Al<sub>2</sub>O<sub>3</sub>(0001) surface<sup>3</sup>. Finally we note in passing that both studies interestingly obtain a rather low site specificity for the formation of OH-groups on the O-rich surface, as in our case expressed by the degenerate surface free energies of the (OH)<sup>br</sup>/O<sup>cus</sup> and O<sup>br</sup>/(OH)<sup>cus</sup> phases. Recalling the large difference in binding energy between O<sup>br</sup> and O<sup>cus</sup>, 2.5 eV vs. 1.2 eV with respect to molecular oxygen<sup>9,10</sup>, this result is rather unexpected.

## VI. SUMMARY

In conclusion we presented the *ab-initio* based surface phase diagram of stable structures of RuO<sub>2</sub>(110) in equilibrium with a humid environment formed of oxygen and water vapor. We find the oxide surface to be completely hydrogenated at room temperature for any realistic gas phase conditions. Depending on the partial pressures in the gas phase H is either present in form of hydroxyl groups at bridge and/or cus sites, or in form of a water-like species at the cus sites of RuO<sub>2</sub>(110). A complete

structural relaxation allowing also for a tilting of the various surface groups was found necessary in order to arrive at the correct relative stabilities of the various phases.

The most notable effect of hydrogen on the oxide surface structure is the stabilization of a polar, O-enriched surface structure through a considerable reduction of the finite dipole moment introduced upon addition of the corresponding terminal oxygen atoms. This finding is analogous to the one of a previous study on the effect of hydrogenation on the stability of the  $\alpha$ -Al<sub>2</sub>O<sub>3</sub>(0001) corundum surface. The lower H-ORu bond strength does however not lead to an instability of the bulk oxide structure, as reflected in the reported negative surface free energies of fully hydroxylated  $\alpha$ -Al<sub>2</sub>O<sub>3</sub>(0001) surfaces under H-rich conditions. Still, the O-H bonds formed on RuO<sub>2</sub>(110) are strong enough that even in UHV annealing temperatures of the order of  $\sim 600$  K will be required to completely remove residual H contaminants from the surface.

For atmospheric gas phase pressure this stability extends roughly up to 1000 K, indicating the necessity to include H as a likely surface species when modeling the function of RuO<sub>2</sub> oxide surfaces in technological applications like e.g. catalysis.

## VII. ACKNOWLEDGEMENTS

This work was partially supported by the Deutsche Forschungsgemeinschaft (Schwerpunkt "Katalyse"). Q.S. is thankful for an Alexander von Humboldt grant. Valuable discussions concerning the experimental preparation of hydrogenated RuO<sub>2</sub>(110) with H. Conrad, A. Lobo, K. Jacobi, J. Wang and C.Y. Fan are gratefully acknowledged.

- 
- <sup>1</sup> V.E. Henrich and P.A. Cox, *The Surface Science of Metal Oxides*, Cambridge Univ. Press, Cambridge (1994).
- <sup>2</sup> C. Noguera, *Physics and Chemistry at Oxide Surfaces*, Cambridge Univ. Press, Cambridge (1994).
- <sup>3</sup> X.-G. Wang, A. Chaka and M. Scheffler, *Phys. Rev. Lett.* **84**, 3650 (2000).
- <sup>4</sup> C.M. Weinert and M. Scheffler, In: *Defects in Semiconductors*, H.J. von Bardeleben (Ed.). *Mat. Sci. Forum* **10-12**, 25 (1986).
- <sup>5</sup> M. Scheffler, In: *Physics of Solid Surfaces - 1987*, J. Koukal (Ed.). Elsevier, Amsterdam (1988).
- <sup>6</sup> E. Kaxiras *et al.*, *Phys. Rev. B* **35**, 9625 (1987).
- <sup>7</sup> G.-X. Qian, R.M. Martin and D.J. Chadi, *Phys. Rev. B* **38**, 7649 (1988).
- <sup>8</sup> X.-G. Wang *et al.*, *Phys. Rev. Lett.* **81**, 1038 (1998).
- <sup>9</sup> K. Reuter and M. Scheffler, *Phys. Rev. B* **65**, 035406 (2002).
- <sup>10</sup> K. Reuter and M. Scheffler, *Phys. Rev. Lett.* (*in press*).
- <sup>11</sup> H. Over *et al.*, *Science* **287**, 1474 (2000).
- <sup>12</sup> Y.D. Kim *et al.*, *Top. Catal.* **14**, 95 (2001).
- <sup>13</sup> L. Zang and H. Kisch, *Angew. Chemie* **112**, 4075 (2000).
- <sup>14</sup> We use  $\mu_{\text{O}}(T, p_{\text{O}_2}) = \frac{1}{2}\mu_{\text{O}_2}(T, p^0) + \frac{1}{2}k_{\text{B}}T\ln(p_{\text{O}_2}/p^0)$  and  $\mu_{\text{H}_2\text{O}}(T, p_{\text{H}_2\text{O}}) = \mu_{\text{H}_2\text{O}}(T, p^0) + k_{\text{B}}T\ln(p_{\text{H}_2\text{O}}/p^0)$  with  $p^0 = 1$  atm and  $\mu_i(T, p^0)$  taken from ref. 15. Experimentally, the critical point of water is at  $T = 647$  K,  $p = 22$  MPa. With these values we obtain  $\mu_{\text{H}_2\text{O}}(647\text{K}, 22\text{MPa}) = -0.91$  eV, which is considered to represent the H<sub>2</sub>O-rich limit of our study.
- <sup>15</sup> D.R. Stull and H. Prophet, *JANAF Thermochemical Tables*, 2nd ed. (Nat. Bureau of Standards, Washington DC, 1971).
- <sup>16</sup> J. Wang *et al.*, *Angew. Chemie Int. Ed.* (submitted).
- <sup>17</sup> P.A. Thiel and T.E. Madey, *Surf. Sci. Rep.* **7**, 211 (1978).
- <sup>18</sup> P. Blaha, K. Schwarz and J. Luitz, **WIEN97**, Techn. Univ. Wien, Austria (1999), ISBN 3-9501031-0-4.
- <sup>19</sup> J.P. Perdew, K. Burke and M. Ernzerhof, *Phys. Rev. Lett.* **77**, 3865 (1996).
- <sup>20</sup> FP-LAPW basis set:  $R_{\text{MT}}^{\text{Ru}} = 1.8$  bohr,  $R_{\text{MT}}^{\text{O}} = 1.0$  bohr,  $R_{\text{MT}}^{\text{H}} = 0.6$  bohr,  $E_{\text{max}}^{\text{wf}} = 20.25$  Ry,  $E_{\text{max}}^{\text{pot}} = 400$  Ry,  $l_{\text{max}}^{\text{wf}} = 12$ ,  $l_{\text{max}}^{\text{pot}} = 6$ , 18 **k**-points in the irreducible part of the  $(1 \times 1)$  BZ.
- <sup>21</sup> *CRC Handbook of Chemistry and Physics*, 81st ed. (CRC Press, Boca Raton FL, 2000).
- <sup>22</sup> N.N. Greenwood, E.J.F. Ross and B.P. Straughan, *Index of vibrational spectra of inorganic and organometallic compounds*, Vol. 1 (Butterworth, London GB, 1972).
- <sup>23</sup> D.D. Wagman *et al.*, *NBS Chemical Thermodynamic Data Base* (Nat. Bureau of Standards, Washington DC, 1965).
- <sup>24</sup> J.P. Perdew and Y. Wang, *Phys. Rev. B* **45**, 13244 (1992).
- <sup>25</sup> C.Y. Fan *et al.*, *J. Chem. Phys.* **114**, 10058 (2001).
- <sup>26</sup> Z.P. Liu, P. Hu and A. Alavi, *J. Chem. Phys.* **114**, 5956 (2001).
- <sup>27</sup> J. Wang *et al.*, *Surf. Sci.* **481**, 113 (2001); *J. Phys. Chem. B* **106**, 3422 (2002).
- <sup>28</sup> Y.D. Kim *et al.*, *J. Phys. Chem.* **105**, 3752 (2001).
- <sup>29</sup> A. Böttcher *et al.*, *J. Phys. Chem. B* **101**, 11185 (1997).
- <sup>30</sup> A. Böttcher and H. Niehus, *Phys. Rev. B* **60**, 14396 (1999).
- <sup>31</sup> A. Böttcher, H. Conrad and H. Niehus, *Surf. Sci.* **452**, 125 (2000).
- <sup>32</sup> K. Reuter and M. Scheffler, (*to be published*).